PAST, PRESENT AND FUTURE OF THE LHCb DETECTOR*

Violetta Cogoni

on behalf of the LHCb Collaboration

Università degli Studi di Cagliari and INFN Cagliari, Italy
and
CERN, 1211 Geneva 23, Switzerland

(Received April 26, 2016)

The LHCb experiment has been designed as a high precision experiment devoted to the search of physics beyond the Standard Model through the study of CP violation and rare decays in hadrons containing b and c quarks. During the Run 1 of LHC, the LHCb detector has performed very well producing a large number of physics results on a vast number of subjects. The first Long Shutdown offered the opportunity to further optimise the detector, anticipating in some cases the interventions foreseen for Run 3. Nevertheless, the phase of upgrade of the detector, foreseen for 2019–2020, will be crucial to exploit the full potential of the LHCb experiment. In this context, an overview of the LHCb detector is presented, concerning its past, present, and foreseen future performances.

DOI:10.5506/APhysPolB.47.1437

1. Introduction

1.1. The LHCb experiment

The LHCb detector [1] is a single-arm forward spectrometer covering the pseudorapidity range of $2 < \eta < 5$, whose structure has been optimised for the study of hadrons containing b and c quarks. The choice of its geometry has been driven by the fact that, at high energy, hadrons from b–$\bar{b}$ pairs are mainly produced in the same forward or backward cone.

The layout of the experiment is reported in Fig. 1. Most sub-detectors are divided in two halves, to allow changes of position for assembly and maintenance purposes, and to access to the beam-pipe. Particles trajectories

* Presented at the Cracow Epiphany Conference on the Physics in LHC Run 2, Kraków, Poland, January 7–9, 2016.

are bended in the horizontal plane by a dipole magnet providing a bending power of about 4 Tm. The VErtex LOcator (VELO) is the tracking subdetector that is placed around the interaction region. The tracking system also includes four planar tracking stations: the Tracker Turicensis (TT) upstream of the magnet, and tracking stations T1–T3 downstream of the magnet. Charged particle identification is achieved by two Ring Imaging Cherenkov Detectors (RICH1 and RICH2), a calorimeter system composed by a Scintillating Pad Detector (SPD), a Preshower (PS), a "shashlik"-type electromagnetic calorimeter (ECAL) and a hadronic calorimeter (HCAL), and a Muon System (M1–M5).

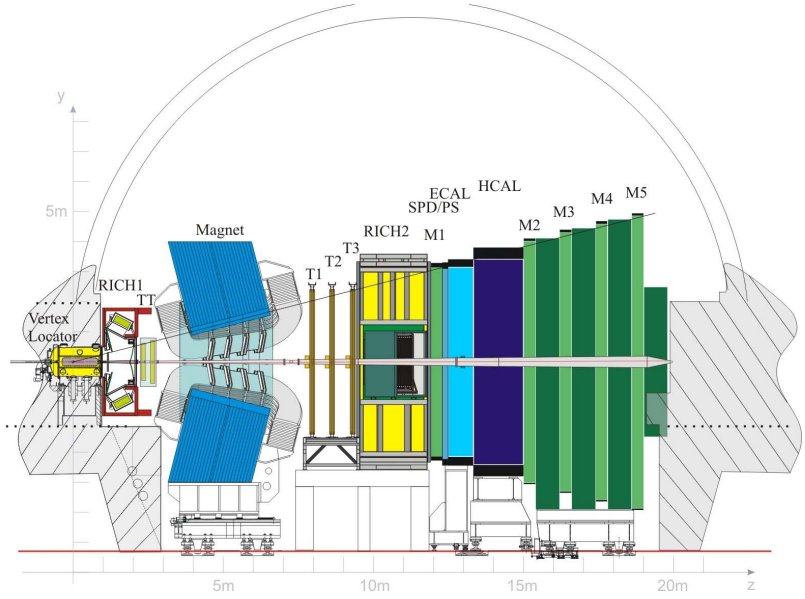


Fig. 1. Two-dimensional view of the LHCb experiment.

Data quality is affected by the pile-up caused by high peaks in luminosity. In order to bring the pile-up under control, LHCb operates at lower (with respect to the other LHC experiments) but levelled luminosity. This operational mode allowed to collect data corresponding to an integrated luminosity of ~ 1 fb^{-1}, ~ 2 fb^{-1}, and ~ 320 pb^{-1} in 2011, 2012, and 2015, respectively.

Excellent resolution is required for an effective separation of the decays of interest from the background. LHCb detectors provide a precise measurement of momentum p, with a relative uncertainty which varies from 0.5% at low momentum p to 1% at 200 GeV/c. This translates into a precise determination of the invariant mass, whose resolution is ~ 8 MeV/c^2 for $B \to J/\psi\, X$ decays, ~ 22 MeV/c^2 for two-body B decays and ~ 100 MeV/c^2

for $B_s \to \phi\,\gamma$. The impact parameter (IP) is measured with a resolution of 20 μm for particles having high transverse momentum p_{T}. Good decay time resolution is important to resolve B_s^0 flavour oscillations and is measured to be 45 fs for $B_s \to J/\psi\,\phi$ and $B_s \to D_s\,\pi$. In addition to this, charged particle identification is essential in any flavour physics programme in order to isolate suppressed decays: LHCb detectors guarantee high efficiency ensuring, at the same time, low particle misidentification: $\varepsilon_e \sim 90\%$ for 5% $P(e \to h)$, $\varepsilon_K \sim 95\%$ for 5% $P(\pi \to K)$, $\varepsilon_\mu \sim 97\%$ for 1–3% $P(\pi \to \mu)$.

1.2. The upgrade of the LHCb detector

The results obtained during Run 1 and Run 2 show that the LHCb detector is working well. Nevertheless, to fully exploit the flavour physics potential, we need to go to very high precision measurements so that the experimental sensitivity reaches the same order of magnitude of the theory uncertainty. This cannot be achieved without upgrading the detector.

The upgraded detector will go beyond the limitations due to the fact that the trigger yield on hadronic events saturates already at 4×10^{32} cm^{-2} s^{-1} (as can be seen in Fig. 2) because of the available bandwidth and the limited discriminating power of the hadronic hardware trigger. The strategy is to increase the luminosity with a detector read-out at 40 MHz with a flexible fully-software trigger which will increase the data rate, so as to collect 50 fb^{-1} during Run 3.

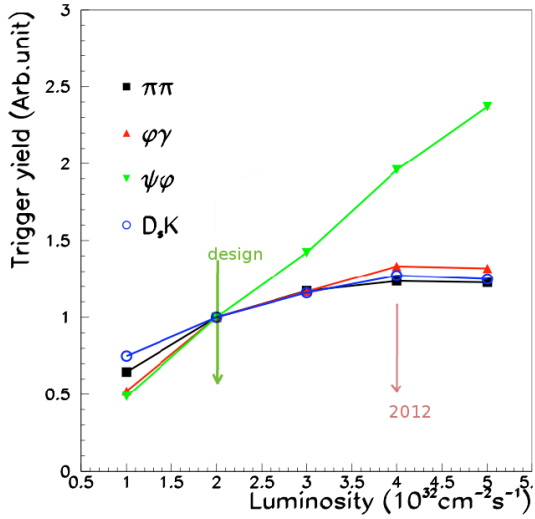


Fig. 2. The trigger yield for four different B mesons decays [2]. Two arrows have been superimposed to point at the current and design luminosity.

The consequence is the necessity to rethink and rebuild the detector front-end electronics (only compatible with the current 1 MHz read-out) and to consolidate the sub-detectors.

2. Trigger

The trigger architecture is split into two levels: the Level-0 (L0) trigger, which is a hardware-implemented trigger; the High Level Trigger (HLT), which consists of a software application running on the CPUs of an event-filter-farm (EFF).

The aim of the L0 trigger is to reduce the rate of the input received by the calorimeters (ECAL, HCAL) and the Muon System to a rate at which the HLT can process the event. During Run 1, in order to optimise the resources use, a fraction of $\sim 20\%$ of L0-accepted events was deferred to disk in order to be processed during the inter-fill time. The HLT is divided into two phases which are executed in sequence: HLT1 which performs a partial event reconstruction; HLT2 where a complete event reconstruction is performed.

The most innovative interventions in Run 2 concerned the trigger. The 20% increase in multiplicity reflects in an increment of the signal, thus the trigger has to be more selective, since the maximum read-out rate is still limited to 1 MHz. In this phase, 100% of the events can be buffered to disk before HLT2 while performing the on-line alignment and calibration of the sub-detectors. The new streaming strategy also allows to only store the candidates for a selection of physics analyses thanks to a direct trigger

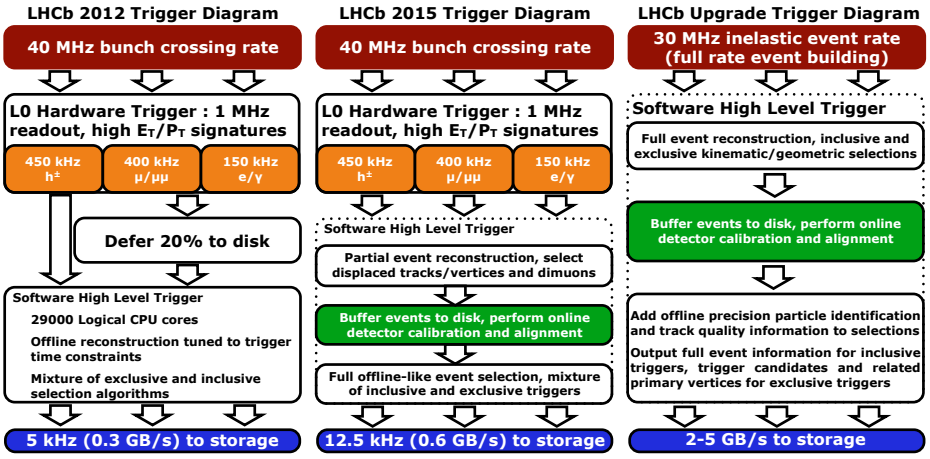


Fig. 3. From left to right, the trigger schemes for Run 1, Run 2, and the foreseen scheme for Run 3 are illustrated.

reconstruction called Turbo stream, with the advantage of reducing the event size of one order of magnitude. Currently, the 20% of the HLT output rate is dedicated to the Turbo stream, and its contribution is foreseen to grow so that after the LHCb upgrade, the majority of the analyses will be sent to it. The upgrade will also allow to go beyond the limitations due to the rate reduction to 1 MHz: the strategy consists in a full 40 MHz readout, with a software-based Low Level Trigger foreseen to replace L0 (which was responsible for the largest inefficiencies in the trigger chain). In this way, the trigger will be as similar as possible to the off-line selection and will have a tunable output rate. In Fig. 3, the evolution of the trigger scheme is depicted.

3. VErtex LOcator

Trajectories of charged particles inside the LHCb detector are reconstructed using dedicated tracking detectors. The VELO is the detector surrounding the interaction region with 42 silicon modules arranged along the beam direction, each providing a measurement of R and ϕ coordinates. Its high spatial resolution enables a precise determination of the particles' flight direction close to the primary interaction, resulting in an excellent IP resolution which reaches $\sigma_{\text{IP}} \sim 20$ μm for high-momentum tracks, as can be seen in Fig. 4.

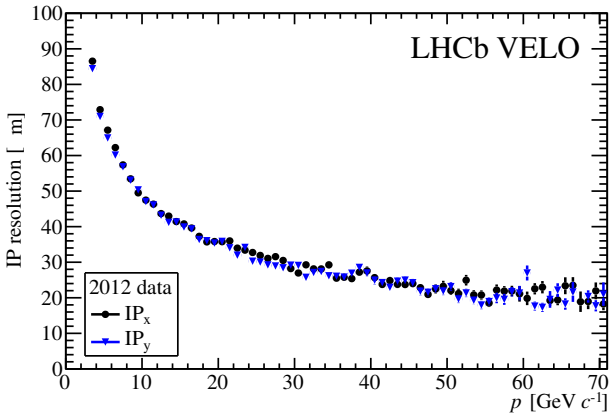


Fig. 4. (Colour on-line) IP$_x$ (black) and IP$_y$ (grey/blue) resolution as a function of momentum determined with data collected in 2012 [3].

During the Run 3 data taking, the VELO will have to maintain and possibly improve its performances; this can only be achieved with a complete replacement of the silicon sensors and of the electronics. The conceptual layout will remain unvaried but the strip technology will be replaced by

pixels of reduced thickness (from 300 to 200 μm) to cope with the increased multiplicity. The expected performances on the IP resolution are reported in Fig. 5, which confirms the expectations about the improvement for Run 3.

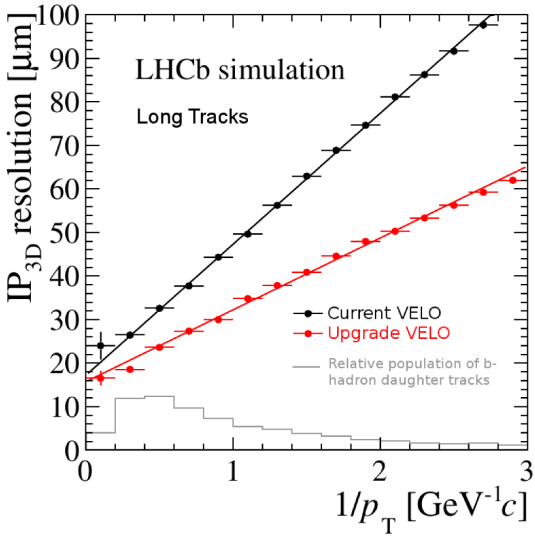


Fig. 5. (Colour on-line) $\mathrm{IP_{3D}}$ resolution for particles reconstructed in all tracking sub-detectors. The current VELO is shown in black circles and the upgraded VELO in grey/red circles, both evaluated at $\nu = 7.6$ and $\sqrt{s} = 14$ TeV. The light grey histogram shows the b-hadron daughter tracks relative population in each bin [4].

4. Tracking system

The LHCb tracking system also includes the Tracker Turicensis (TT), a large area silicon strip detector, placed upstream of the magnet, and three T stations, placed downstream of the magnet, consisting of a silicon-based inner part, the Inner Tracker (IT), and of an Outer Tracker (OT) of straw tubes. Each sub-detector consists of four detection planes rotated by a stereo angle of $0°/+5°/-5°/0°$.

The reconstruction of high-multiplicity B decays demands high efficiency on the single hit and the possibility to determine the hit position with high precision. The efficiency on the single hit is above 99% for all the tracking stations ($\varepsilon_{\mathrm{hit}} \approx 99.8\%$, 99.9%, and 99.2% for TT, IT, and OT, respectively); the resolution on the hit position is $\sigma_{\mathrm{hit}} = 53$ μm for TT and 54 μm for IT while it is of ≈ 200 μm for the OT, where the requirements on the resolution are relaxed.

The performances of all the sub-detectors of the tracking system have been satisfying during Run 1 and Run 2. Nevertheless, the TT has to be replaced for the upgrade for three main reasons:

— it is not sufficiently radiation hard;

— in order to reduce the costs of read-out electronics, the read-out of four consecutive sensors is bounded together to form strips, and this will lead to unacceptably high occupancy at high luminosity;

— the integrated Beetle front-end chip is not compatible with the 40 MHz read-out and cannot be replaced without damaging the module.

The TT will be substituted by the Upstream Tracker (UT), which will still consist of four planes of silicon strips. The improvements include thinner sensors (from 500 μm to 250 μm) with finer segmentation (see Fig. 6) and larger angular coverage, thanks to circular cut-outs on the UT planes. In addition to this, the signal will be processed at the sensors rather than being taken out with long cables, allowing to reduce the electronic noise. The UT hits will be fundamental for the rejection of ghost tracks. The requirement to have three or more UT hits on tracks reconstructed in all particles sub-detectors (*long* tracks) is expected to reduce the ghost track rate of a factor 2–4, as can be seen in Fig. 7.

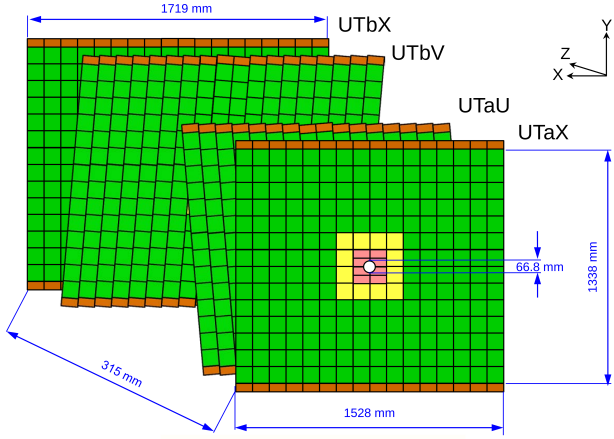


Fig. 6. (Colour on-line) Layout of the UT looking downstream. Different sensor segmentations are colour coded: 95 μm $\times$ 4.9 cm (grey/red), 95 μm $\times$ 9.7 cm (light grey/yellow), 190 μm $\times$ 9.7 cm (dark grey/green) [5]. The values here reported can be compared to the current TT segmentation 183 μm (x)$\times$4.9 cm (y).

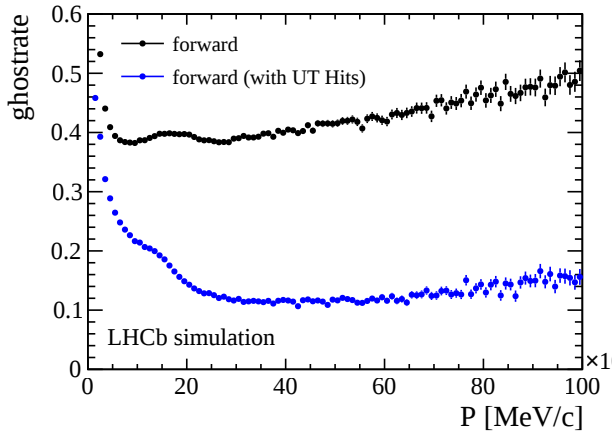


Fig. 7. Ghost rate for *long* tracks with and without the requirement of at least three UT hits, reported as a function of momentum for a sample of simulated $B_s \to \phi\phi$ events at an interaction rate of $\nu = 7.6$ [5].

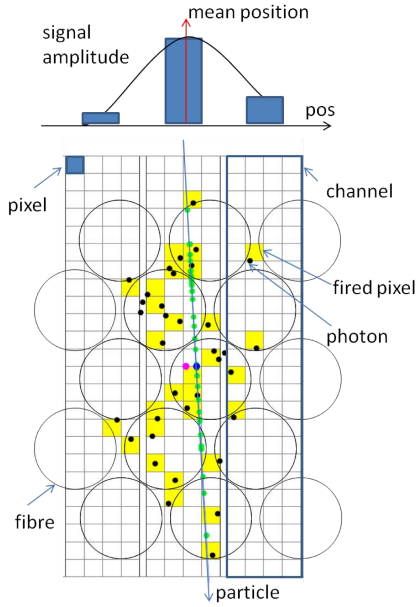


Fig. 8. The ionising particle produces photons in the fibres along its trajectory. These photons are propagated to the fibre and then collected on the SiPM photodetectors. Each pixel can detect one photon, thus the signal is proportional to the number of hit (coloured) pixels [5].

The T station geometry was chosen so that the maximum occupancy of the OT in the external region was limited to 10% at design luminosity. Improvements have already been made to be able to collect data at an instantaneous luminosity of 5×10^{32} cm^{-2} s^{-1} with a maximum occupancy of 25%. Nevertheless, at upgrade luminosity, the occupancy will definitely be intolerable. The solution is to replace the modules with 2.5 m long and 250 μm thick scintillating fibers, which allow optical signal transportation outside the acceptance volume, read-out by Silicon Photonmultipliers (SiPMs). The new modules will be hosted in three stations of four layers each, rotated by a stereo angle of $0°/+5°/-5°/0°$, with a circular hole to account for the beam-pipe structure. The features of the signal in the modules have been studied through a realistic simulation in order to evaluate the hit detection efficiency and spatial resolution. The signal generation is illustrated in Fig. 8. The new Scintillating Fiber Tracker (SciFi Tracker) has been designed to reach an efficiency on the single hit ε_{hit} of about 99% and a resolution on the single hit on the bending plane σ_{hit} of about 100 μm.

5. Ring Imaging CHerenkov detectors

The primary role of the RICH system is the identification of charged hadrons but it also contributes to the identification of charged leptons. The two sub-detectors cover different angular and momentum ranges:

— RICH 1, placed upstream of the magnet, is designed to identify particles in the momentum range of 2 GeV/c<p<40 GeV/c in the angular region 25 mrad–300 mrad;

— RICH 2, placed downstream of the magnet, is optimised for the identification of particles in the momentum range of 30 GeV/c<p<100 GeV/c in the angular region 15 mrad–120 mrad.

Particles traversing the radiators produce Cherenkov rings on a plane of Hybrid Photon Detectors located outside acceptance. Solitary rings can be unambiguously associated to a single and isolated track, and for this reason, they provide a useful test of RICH performances. In Fig. 9, the reconstructed Cherenkov angle as a function of momentum is shown using isolated tracks, and the bands corresponding to different masses are clearly visible and separated.

The RICH particle identification performance on data has been studied in the control samples $K^0_s \to \pi^+\pi^-$, $\Lambda \to p\pi^-$, and $D^{*+} \to D^0(K^-\pi^+)\pi^+$ for π, K and p tracks. The performances for kaon efficiency (kaons identified as kaons) and pion misidentification fraction (pions misidentified as kaons) is shown in Fig. 10 as a function of momentum for data and simulation. Results

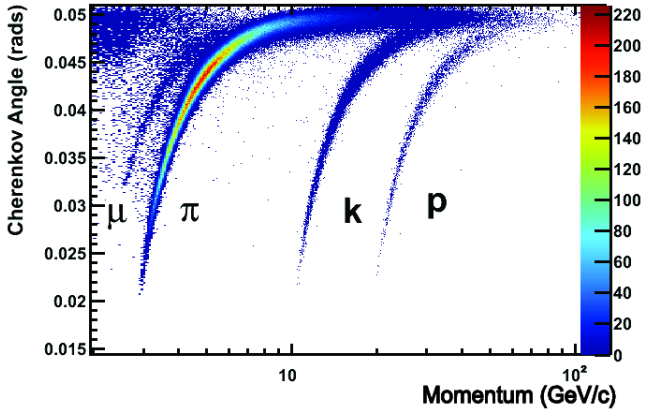


Fig. 9. Reconstructed Cherenkov angle for isolated tracks as a function of track momentum. The bands for muons, pions, kaons, and protons are clearly observable [6].

are shown with two different cuts on PID, one optimising the efficiency and the other maximising the pion rejection fraction: in the first case, a likelihood for the kaon hypothesis larger than that for the pion hypothesis is required, *i.e.* $\Delta \log \mathcal{L}(K-\pi) > 0$, and this results in a kaon efficiency of $\approx 95\%$ with a pion misidentification fraction of $\approx 10\%$; in the second case, a stricter requirement is used on PID, $\Delta \log \mathcal{L}(K-\pi) > 5$, and this reduces the pion misidentification fraction to $\approx 3\%$ with a modest reduction in kaon efficiency to $\approx 90\%$. These values are averaged over the momentum range of 2–100 GeV/c. For all the distributions, a good agreement data-simulation is clear.

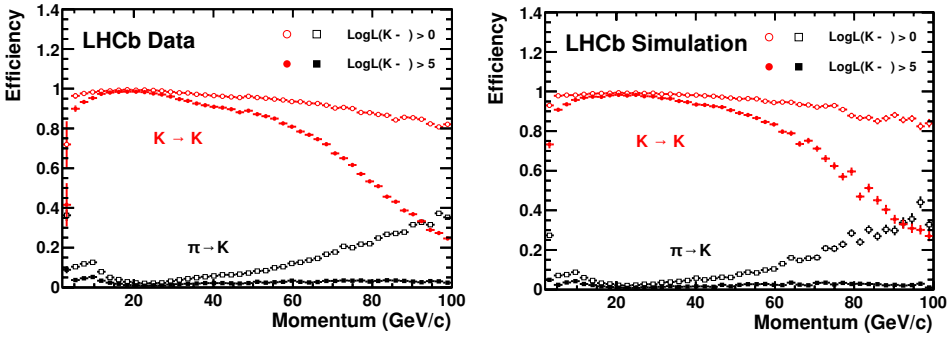


Fig. 10. Kaon identification efficiency and pion misidentification fraction in data (left) and simulation (right) as a function of momentum. Two different PID requirements have been imposed on the sample, resulting in open and filled marker distribution [6].

The overall structure will remain unchanged for the upgrade with significant modification only for RICH 1, whose optical layout has to be modified to reduce the large foreseen occupancy in the central region of the detector. To halve the occupancy, the focal length of the spherical mirrors will be increased by a factor of $\approx \sqrt{2}$. To restore the focusing, the spherical mirror radius of curvature will also increase. The foreseen changes will also improve the Cherenkov angle resolution reducing the aberrations of the spherical mirrors. The differences introduced in the geometry are visible from the comparison of Fig. 11 (a) and (b).

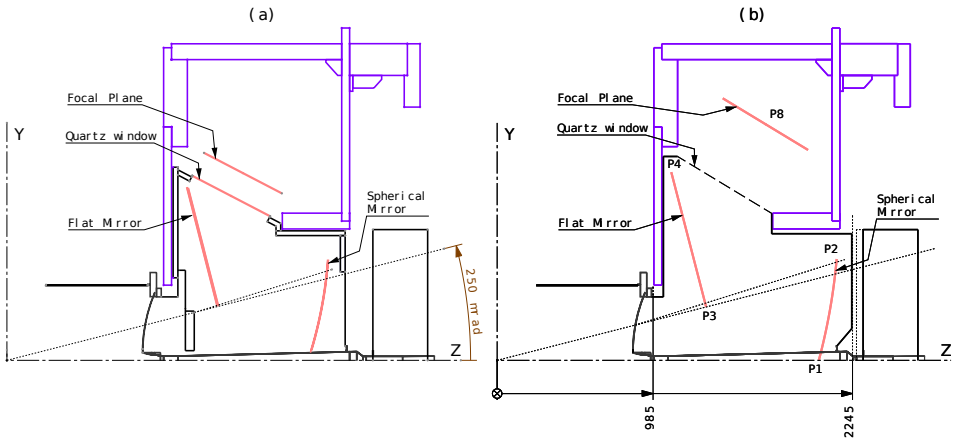


Fig. 11. Layout of the optical geometry of the current (a) and upgraded (b) RICH1 sub-detector [7].

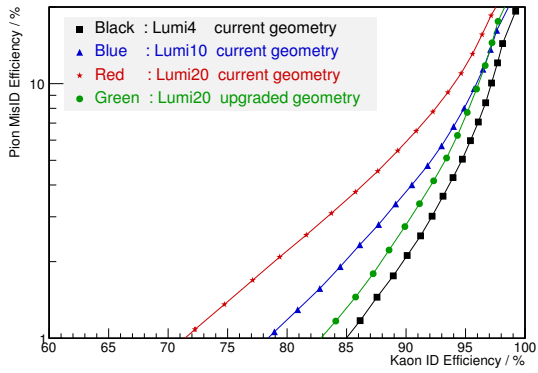


Fig. 12. Particle identification performances of the current geometrical layout for the instantaneous luminosities of 3.9×10^{32} (Lumi4), 10×10^{32} (Lumi10), 20×10^{32} (Lumi20). The performances corresponding to Lumi20 with the upgraded geometry are also reported [7].

In Fig. 12, the particle identification performance is shown for the current geometry at three luminosities, and is compared to the performance for the upgraded geometry at the instantaneous luminosity of 20×10^{32} cm^{-2} s^{-1}. As the luminosity increases, the plot shows a loss in performance that is mostly recovered when using the new RICH 1 geometry.

6. Calorimeters

The Calorimeter system includes: a Scintillating Pad Detector (SPD), used to identify charged particles for e/γ separation; a PreShower (PS), used to identify electromagnetic particles; an Electromagnetic Calorimeter (ECAL) with a "shashlik" geometry of 2 mm lead sheets and 4 mm scintillator plates; a Hadronic Calorimeter (HCAL) consisting of thick (16 mm) iron and 4 mm scintillating tiles arranged parallel to the beam. The performances of high-energy photon reconstruction are illustrated by Fig. 13 where the mass resolution for the signal $B^0_d \to K^{*0}\gamma$ is dominated by ECAL energy resolution, which can be calculated as $\sigma(E)/E = 10\%/\sqrt{E} + 1.5\%$ (with E in GeV) thus being of $\approx 2\%$ for 93 MeV/c^2.

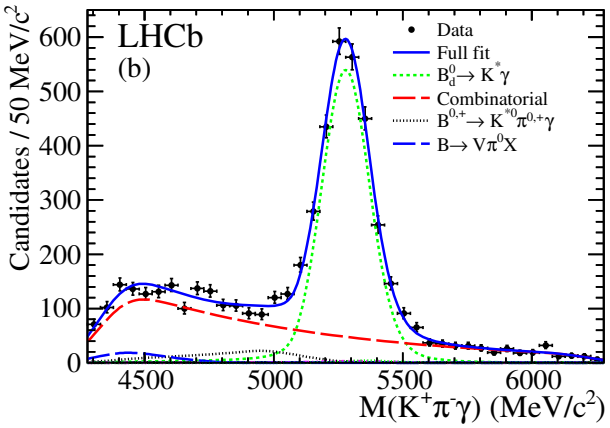


Fig. 13. Invariant mass distribution of $B^0 \to K^{*0}\gamma$ decay candidates [8].

During Run 1 and Run 2, the Calorimeter system performed well despite the decision to operate at higher luminosity than foreseen during the design period. In view of Run 3, the removal of SPD/PS is foreseen, since their principle purpose is in the L0 trigger and the future LLT will not have to achieve the same level of suppression, hence the requirements are relaxed. This will simplify the Calorimeter design with great advantages in terms of calibration and project costs. On the contrary, ECAL and HCAL modules will remain mostly unchanged. The current PMTs will be kept reducing the gain of a factor of 5 to keep the same mean anode current as today. As usual,

the new readout at 40 MHz will require new design of the front-end and back-end electronics. Radiation damage studies showed a sizeable degradation for the innermost modules of HCAL, but they are not expected to remain operational for the full-life span of the upgrade. The eventual loss of HCAL central cells is expected not to impact upon the physics performance of the experiment. ECAL modules are expected to be able to remain operational up to an integrated luminosity of ~ 20 fb^{-1} so the replace of the most irradiated modules is only foreseen for the third Long Shutdown of the LHC.

7. Muon system

The importance of an efficient and effective muon identification is related to the fact that many key decay channels for the physics programme of LHCb have muons in the final state. The present muon system consists of five stations (M1–M5), interspersed with iron filters, each divided into four concentric regions (R1–R4) equipped with Multi-Wire Proportional Chambers (MWPCs), with the exception of M1R1, which hosts triple-GEM detectors. In the Muon System, the off-line selection of muons starts from a coincidence of the stations (IsMuon) and a discriminating variable (muDLL) is subsequently used. This procedure guarantees high efficiency for the identification of muons ensuring, at the same time, low pion misidentification fraction, as can be seen in Fig. 14. Being the most shielded sub-detector, the muon system will tolerate the particle rates up to an instantaneous luminosity of 2×10^{33} cm^{-2} s^{-1} at the collision energy of 14 TeV in all stations apart from M1, which will not be used during Run 3; nevertheless, also the particle flux in the innermost region of M2 is expected to be very high, and so the installa-

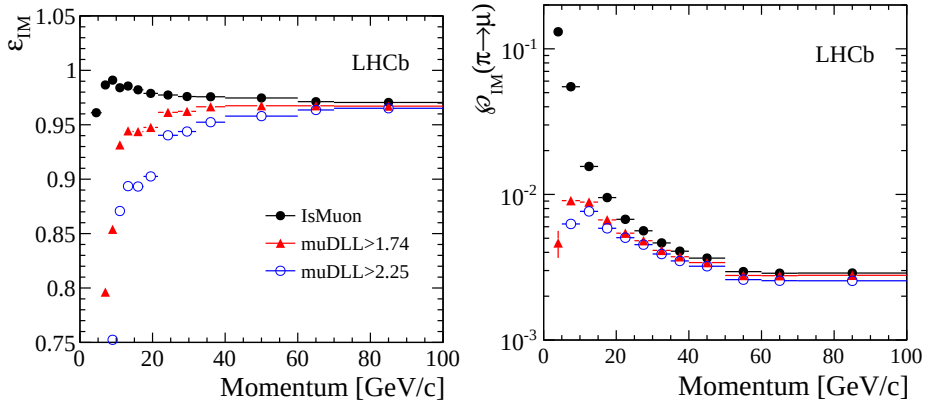


Fig. 14. Muon identification efficiency (left) and pion misidentification fraction (right) as a function of momentum in the Muon System for the Boolean variable IsMuon and for two different cuts on the discriminating variable muDLL.

tion of additional shielding around the beam-pipe in front of M2 is foreseen. Finally, the currently installed front-end electronics is already read-out at the rate of 40 MHz but the off-detector read-out electronics only provides information at the limited rate of 1 MHz, and so the current Off Detector Electronics (ODE) will be substituted by the new Off Detector Electronics (nODE) based on a new radiation tolerant custom ASIC, the nSYNC, whose prototype is currently under test. In addition to these structural changes, a new algorithm based on multivariate analysis has been developed which is able to restore the pion rejection performance at high pile-up conditions.

8. Conclusions

The LHCb detector has performed excellently during Run 1. The detector performances in Run 2 are similar to those observed during the first data taking run, and are improving thanks to major changes in the trigger strategy, with great advantages for an increasing number of analyses. All the Technical Design Report for the Upgrade have been approved and the projects for the Run 3 are progressing with the first prototypes under test. During Run 3, LHCb will make a full use of the Turbo stream thanks to the success of the on-line alignment and calibration.

REFERENCES

[1] The LHCb Collaboration, *JINST* **3**, S08005 (2008).

[2] The LHCb Collaboration, Letter of Intent for the LHCb Upgrade, Technical Report CERN-LHCC-2011-001, LHCC-I-018, CERN, Geneva, March 2011.

[3] R. Aaij *et al.*, *JINST* **9**, 09007 (2014).

[4] The LHCb Collaboration, LHCb VELO Upgrade Technical Design Report, Technical Report CERN-LHCC-2013-021, LHCB-TDR-013, CERN, Geneva, November 2013.

[5] The LHCb Collaboration, LHCb Tracker Upgrade Technical Design Report, Technical Report CERN-LHCC-2014-001, LHCB-TDR-015, CERN, Geneva, February 2014.

[6] R. Aaij *et al.*, *Int. J. Mod. Phys. A* **30**, 1530022 (2015).

[7] The LHCb Collaboration, LHCb PID Upgrade Technical Design Report, Technical Report CERN-LHCC-2013-022, LHCB-TDR-014, CERN, Geneva, November 2013.

[8] R. Aaij *et al.*, *Nucl. Phys. B* **867**, 1 (2013).